Interstitial cells of Cajal in *W*^{sh}*/W*^{sh} *c-kit* mutant mice

Satoshi IINO[1], Satomi HORIGUCHI[1], Kazuhide HORIGUCHI[1] and
Takashi HASHIMOTO[1]

[1]*Department of Anatomy, University of Fukui Faculty of Medical Sciences, Eiheiji,*
 Fukui 910-1193, Japan

Abstract

The c-Kit receptor tyrosine kinase regulates the development and differentiation of several progenitor cells. In the gastrointestinal (GI) tract, the c-Kit regulates the development of the interstitial cells of Cajal (ICC) that are responsible for motility regulation of the GI musculature. *W-sash* (W^{sh}) is an inversion mutation upstream of the *c-kit* promoter region that affects a key regulatory element, resulting in cell-type-specific altered gene expression, leading to a decrease in the number of mast cells, melanocytes, and ICC. We extensively examined the GI tract of W^{sh}/W^{sh} mice using immunohistochemistry and electron microscopy. Although the musculature of the W^{sh}/W^{sh} mice did not show any c-Kit immunoreactivity, we detected intensive immunoreactivity for transmembrane member 16A (TMEM16A, anoctamin-1), another ICC marker. TMEM16A immunopositive cells were observed as ICC-MY in the gastric corpus-antrum and the large intestine, ICC-DMP in the small intestine, and ICC-SM in the colon. Electron microscopic analysis revealed these cells as ICC from their ultrastructural features, such as numerous mitochondria and caveolae, and their close contact with nerve terminals. In the developmental period, we examined 14.5 and 18.5 day embryos but did not observe c-Kit immunoreactivity in the W^{sh}/W^{sh} small intestine. From this study, ICC subtypes developed and matured structurally without c-Kit expression. W^{sh}/W^{sh} mice are a new model to investigate the effects of c-Kit and unknown signaling on ICC development and function.

Key words: gastrointestinal tract, c-Kit, TMEM16A, *W* mutation, ICC

Introduction

The c-Kit receptor tyrosine kinase is encoded at the *Dominant White Spotting* (*W*) locus on chromosome 5 of mice (1, 2) and belongs to the platelet-derived growth factor and colony-stimulating factor 1 receptor family. In several progenitor cells, c-Kit regulates hematopoiesis, gametogenesis, and melanogenesis, as well as the

proliferation of mast cells and interstitial cells of Cajal (ICC) (3, 4). *W* mutant mice with several spontaneous mutations in the *c-kit* gene have loss of function of the c-Kit, showing various phenotypes, such as anemia, infertility, diminished coat color, decreased mast cells, and depleted ICC numbers. The *W* mutation is a null mutation, which induces the deletion of the transmembrane domain of the c-Kit protein. Moreover, the W^v mutation is a point mutation in the c-Kit kinase domain, resulting in impaired kinase activity. *W-sash* (W^{sh}) is an inversion mutation upstream of the *c-kit* promoter region, which affects a key regulatory element, resulting in cell-type-specific altered gene expression (5). W^{sh} mutant mice are fertile and non-anemic, different from other *W* mutants, although this mutation reduces c-Kit kinase activity (6). A recent study revealed that W^{sh} mice lacked mast cells, melanocytes, and ICC and are thought to be a new model for c-Kit function research (7).

ICC are gastrointestinal (GI) mesenchymal cells that specifically express c-Kit and form a cellular network within the GI musculature (4, 8, 9). ICC contribute to GI motility regulation by generating slow waves and transducing neural inputs to smooth muscles (4). ICC are classified into several subtypes according to their morphology and distribution patterns in the GI musculature. ICC-MY are multipolar-shaped cells in the myenteric layer through the GI tract, whereas ICC-IM are bipolar-shaped cells in circular and longitudinal muscle layers. ICC-DMP are a specific type of ICC-IM in the circular muscle layer of the small intestine. ICC-SM are multipolar-shaped with thin processes and are located in the submucosal border of the colonic muscle layers. The GI tract of animals with an altered c-Kit signaling does not possess the ICC subtypes, since ICC development and differentiation depends on the signals from c-Kit and c-Kit ligand (stem cell factor, SCF) (9, 10). For example, W/W^v, W^v/W^v, and W^{jic}/W^{jic} mice that have *c-kit* gene mutations and inadequate c-Kit kinase activity are ICC-MY-deficient (9–13). Similarly, SCF-deficient Sl/Sl^d mice that have impaired c-Kit signaling show defects in ICC-MY (10, 14). However, our recent study using several mutant mice revealed that ICC-DMP were independent of c-Kit signaling and were observed as normal based on their developmental stage (15). These findings suggest that ICC subtypes can develop and differentiate without c-Kit signaling. We previously showed ICC-DMP with neurokinin 1 receptor (NK1R) immunoreactivity in W^{sh}/W^{sh} mice (16), although these mice have been reported to show defects in c-Kit immunoreactivity throughout the GI tract in their early stages to adulthood (7). In this study, we examined the GI musculature using immunohistochemical reactivity to TMEM16A (Transmembrane member 16A, anoctamin-1), a general marker of ICC (17–19), and using electron microscopy to characterize the ultrastructure, to determine whether W^{sh}/W^{sh} mice have ICC subtypes without c-Kit expression.

Methods

C;B6-a/a-b/b-W^{sh}/W^{sh} mice (RBRC00762) were provided by RIKEN BRC (Japan), which participates in the National Bio-Resource Project of MEXT, Japan. Both W^{sh}/W^{sh} and BALB/c mice (Japan SLC) were maintained in our laboratory. The studies were performed on male mice aged 8–12 weeks (n=20 W^{sh}/W^{sh} mice, n=5 BALB/c mice) and both 14.5 day (E14.5) and 18.5 day embryos (E18.5) (n=3 each mice). The use and treatment of the animals were in accordance with the Guidelines for Animal Experiments, the Regulations for Animal Research at University of Fukui. All efforts were made to minimize the number and suffering of animals used in this study.

The GI tract was flushed with 0.01 M phosphate-buffered saline (PBS, pH 7.2) before being pinned to the Sylgard elastomer floor of a dissecting dish for the cryosections and the whole mount preparations (15, 20). Then, the samples were fixed with Zamboni's fixative (2% paraformaldehyde prepared in a 1.5% saturated picric acid solution with a 0.1 M phosphate buffer, pH 7.3) for 2 h at room temperature. After fixation, the tis-

sues were cut into 10-μm thick sections using a cryostat apparatus. The muscular whole mounts were obtained by removing the mucosa. The specimens were pre-incubated with normal donkey serum (5% in PBS) for 1 h. Then, the specimens were incubated overnight with the following antibodies: rat anti-c-Kit (ACK4; 1:700; ACL8936AP; Cedarlane), goat anti-c-Kit (1:1,000; AF1356, R&D), rabbit anti-TMEM16A (1:400; ab53212; Abcam), rat anti-platelet derived growth factor receptor alpha (PDGFRα, APA5; 1:500; 14-1401; eBioscience), and mouse anti-alpha smooth muscle actin (SMA)-Cy3 (1:3,000; 1A4, C6198; Sigma-Aldrich). After incubation with the aforementioned primary antibodies, they were washed with PBS before being incubated with Alexa Fluor-coupled donkey anti-IgG (1:500; Molecular Probes, USA), a secondary antibody, for 1 h. Then, the specimens were washed with PBS and counterstained with 4′,6-diamidino-2-phenylindole (DAPI; Molecular Probes) and mounted in Anti-Fade Fluorescence Mounting Medium-Aqueous, Fluoroshield (ab104135, Abcam). The fluorescent images were examined at excitation wavelengths of 350 nm, 488 nm, and 543 nm using a Leica TCS-SP2 confocal microscope (Leica Microsystems). The images were collected and composed using the Leica Confocal Software, and Adobe Photoshop CS6 (Adobe Systems, USA) was used to compose the final plates.

The absence of an observable non-specific immunoreaction was confirmed by incubating the sections with normal rat, rabbit or goat serum instead of the primary antibody and then with the secondary antibody.

For conventional electron microscopy (20, 21), tissues from the three mutants were fixed using a solution containing 3% glutaraldehyde and 4% paraformaldehyde in a 0.1 M phosphate buffer, pH 7.2, for 2 h at room temperature. These specimens from stomach, ileum and proximal colon were post-fixed with 1% OsO_4 in PB, block-stained with a uranyl acetate solution, and embedded in Epon 812. The ultrathin sections were stained with uranyl acetate and lead citrate and examined under an electron microscope (Hitachi H-7650).

Results

We investigated the sections and whole mount preparations to identify all ICC types. Consistent with published results (11), c-Kit immunopositive cells were observed from throughout the stomach to the colon in BALB/c mice. In the W^{sh}/W^{sh} mice, c-Kit immunopositive cells examined by antibodies ACK4 (20) or AF1356 (22) were not observed. We used an antibody to TMEM16A, another marker to examine ICC, which was reported as a suitable antibody for investigating ICC in W mutant mice (23). In the stomach, BALB/c mice had ICC-IM and ICC-MY that showed c-Kit and TMEM16A immunoreactivities (Fig. 1A and C). The stomach of W^{sh}/W^{sh} mice did not show c-Kit immunoreactivity but had TMEM16A immunoreactivity at the myenteric layer in the gastric corpus and antrum (Fig. 1B and D). TMEM16A immunopositive cells were examined using whole mount preparations and found to have multipolar shaped cells at the myenteric layer of the gastric corpus, that is, ICC-MY (Fig. 3A and B). The density of ICC-MY of W^{sh}/W^{sh} mice gradually increased from the corpus to the antrum and was less than that of BALB/c mice. On the other hand, ICC-IM were not detected by TMEM16A immunoreactivity. In the small intestine of BALB/c mice (Fig. 1E), ICC-DMP in the circular muscle and ICC-MY at the myenteric layer showed c-Kit and TMEM16A immunoreactivities. In the small intestine of W^{sh}/W^{sh} mice (Fig. 1F), TMEM16A immunoreactivity was only observed in the circular muscle as ICC-DMP. TMEM16A immunopositive ICC-DMP (Fig. 3C) were bipolar-shaped and slender, as known in c-Kit immunopositive ICC-DMP or NK1R immunopositive ICC-DMP (16). In the cecum of BALB/c mice (Fig. 2A), both ICC-IM and ICC-MY were observed to be c-Kit and TMEM16A immunopositive. In the cecum of W^{sh}/W^{sh} mice (Figs. 2B and 3D), there were TMEM16A immunopositive cells that showed a multipolar shape with long processes at the myenteric layer typical of ICC-MY. In the colon of BALB/c mice (Fig. 2C and E),
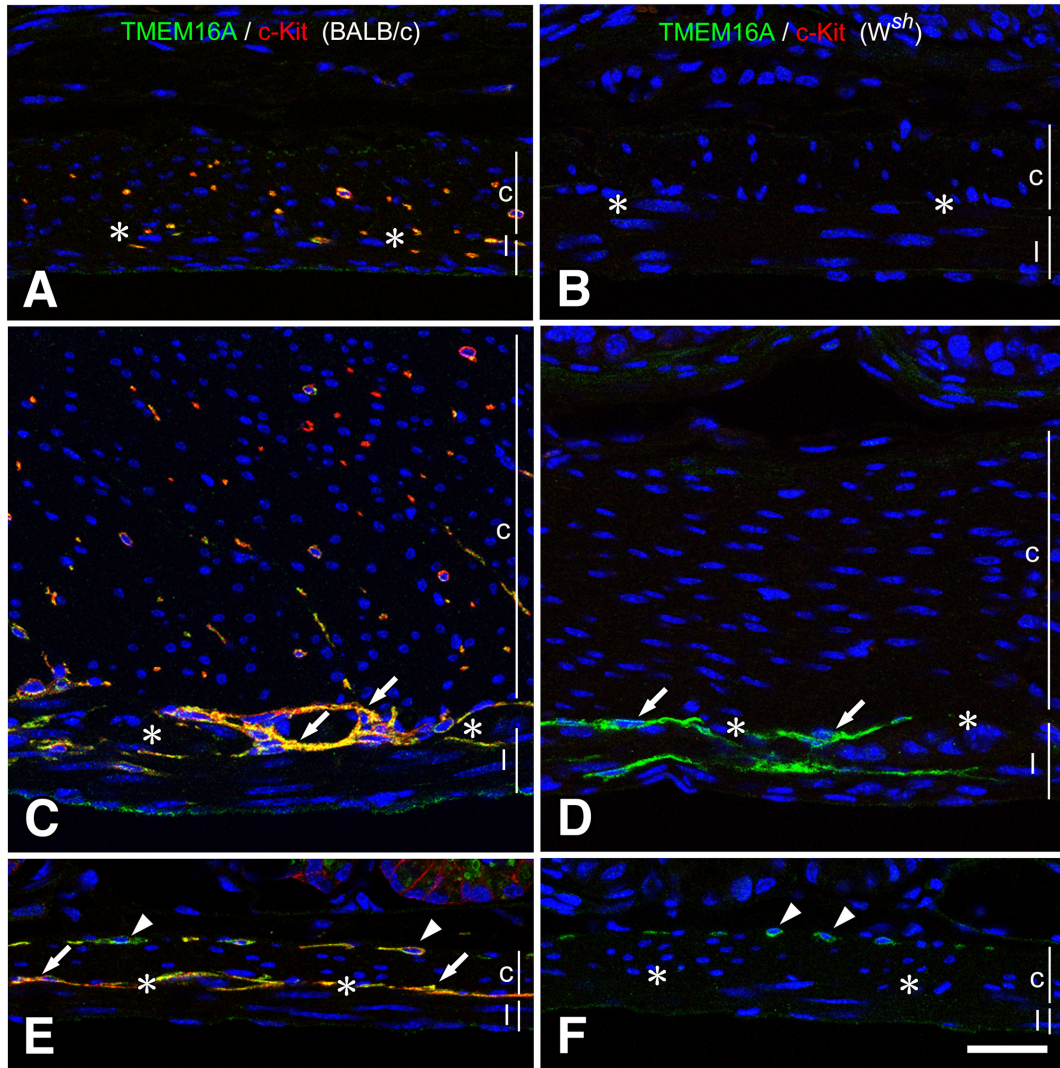
Fig. 1. Musculature of the stomach and small intestine of BALB/c and W^{sh}/W^{sh} mice.
ICC were detected using immunofluorescence, showing TMEM16A immunoreactivity (green) and c-Kit ACK4 immunoreactivity (red) in both BALB/c (A, C, E) and W^{sh}/W^{sh} (B, D, F) mice. In the fundus (A, B), ICC-IM were observed in the musculature only in BALB/c mice. In the corpus (C, D), BALB/c mice have ICC-MY (arrows) and ICC-IM. Contrastingly, W^{sh}/W^{sh} mice have only ICC-MY (arrows) that were confirmed through TMEM16A immunoreactivity. In the small intestine (E, F), BALB/c mice have ICC-DMP (arrowheads) and ICC-MY (arrows) with TMEM16A (green) and c-Kit (red) immunoreactivities, whereas W^{sh}/W^{sh} mice have TMEM16A immunopositive ICC-DMP (arrowheads) in the circular muscle. c and l represent circular and longitudinal muscle layers, respectively. Asterisks show myenteric layer. Bar: 50 μm.

ICC-SM, ICC-IM, and ICC-MY were observed to have both c-Kit and TMEM16A immunoreactivities. In the colon of W^{sh}/W^{sh} mice (Fig. 2D and F), TMEM16A immunopositive cells were distributed at the submucosal border of the circular muscle and myenteric layer. At the submucosal border (Fig. 3E), TMEM16A immunopositive cells were bipolar-shaped with multiple short processes typical of ICC-SM. At the myenteric layer of the proximal colon (Fig. 3F), TMEM16A immunopositive cells were multipolar-shaped with several thin processes and formed a cellular network, which is characteristic of ICC-MY. The density of ICC-MY of W^{sh}/W^{sh} mice was less than that of BALB/c mice.

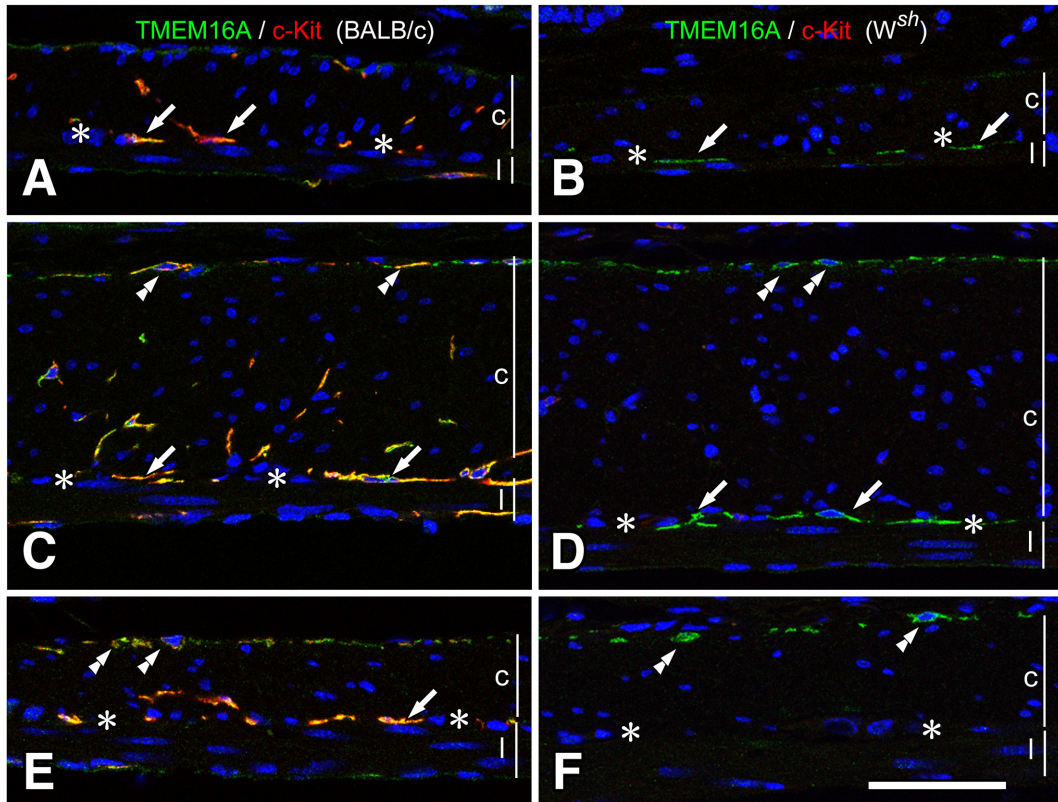In the GI musculature, there are two types of interstitial cells: ICC that have both c-Kit and TMEM16A

Fig. 2. Musculature of the large intestine of BALB/c and W^{sh}/W^{sh} mice.
ICC were observed through immunofluorescence, showing TMEM16A immunoreactivity (green) and c-Kit ACK4 immunoreactivity (red) in both BALB/c (A, C, E) and W^{sh}/W^{sh} (B, D, F) mice. In the cecum (A, B), ICC-IM and ICC-MY (arrows) in BALB/c mice were observed to have TMEM16A and c-Kit immunoreactivities, and only ICC-MY (arrows) in W^{sh}/W^{sh} mice were observed to have TMEM16A immunoreactivity. In the proximal colon (C, D), ICC-SM (double arrowheads) and ICC-MY (arrows) showed TMEM16A immunoreactivity in W^{sh}/W^{sh} mice. In the distal colon (E, F), ICC-SM (double arrowheads) exhibited TMEM16A immunoreactivity in W^{sh}/W^{sh} mice. c and l represent circular and longitudinal muscle layers, respectively. Asterisks show myenteric layer. Bar: 50 μm.

immunoreactivities and fibroblast-like cells (FLC) that have PDGFRα immunoreactivity (24). FLC were distributed in the muscle layers and myenteric layer and often stood alongside ICC. Throughout the GI tract, W^{sh}/W^{sh} mice had FLC similar to BALB/c mice tissues, despite the deficiency of ICC subtypes (Fig. 4).

Using an electron microscope, we examined the GI musculature of all samples from three W^{sh}/W^{sh} mice and obtained same results. In the gastric corpus (Fig. 5A and B), ICC-MY were slender and possessed many caveolae in the myenteric layer. There was no ICC-IM in the musculature of the circular and longitudinal layers. In the small intestine (Fig. 5C and D), ICC-DMP were observed to be closely associated with nerve fiber bundles. It was also noted that ICC-MY were not observed around myenteric ganglia. In the colon (Fig. 5E-G), ICC were observed at the submucosal surface of the circular muscle layer as ICC-SM and at the myenteric layer as ICC-MY. Moreover, ICC-IM were not identified in the muscle layers.

It is known that c-Kit regulates ICC development and differentiation in the embryonic and postnatal period (9). We examined BALB/c and W^{sh}/W^{sh} mice embryos and c-Kit immunoreactivity during the embryonic stage. In E14.5, in the small intestine (Fig. 6A and B), c-Kit immunoreactivity was observed at the myenteric and longitudinal muscle layers but was negative for actin immunoreactivity in BALB/c mice; this is consisted with the report of Torihashi et al. (25). In contrast, c-Kit immunoreactivity was not observed in the muscu-
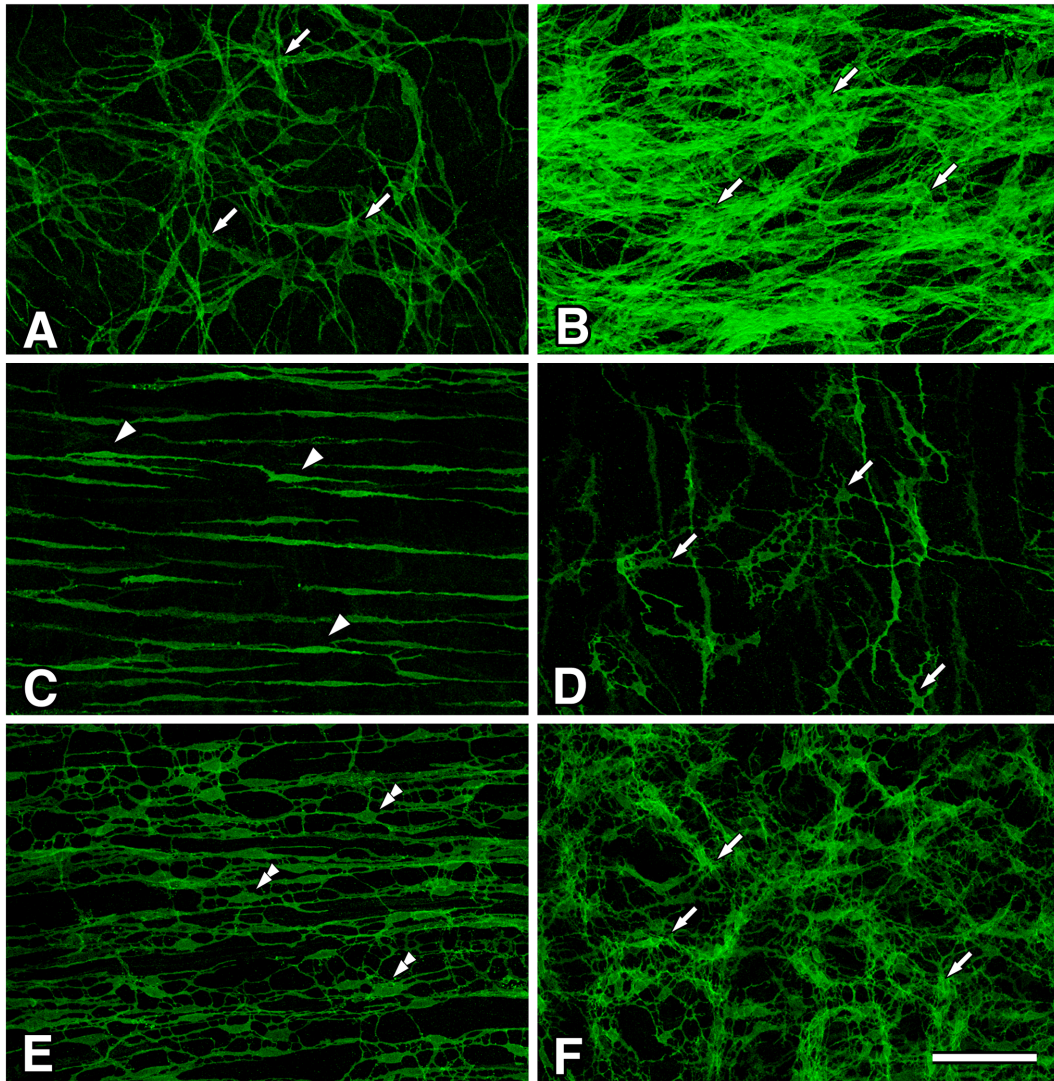
Fig. 3. Whole mount preparations of W^{sh}/W^{sh} mice musculatures.
ICC were detected to have TMEM16A immunoreactivity in the gastrointestinal musculature. In the gastric corpus (A), ICC-MY (arrows) were observed to have multipolar shape in the myenteric layer. In the gastric antrum (B), ICC-MY (arrows) showed a multipolar shape and existed under crowded circumstances in the myenteric layer. In the small intestine (C), ICC-DMP (arrowheads) in the circular muscle layer were observed to have a bipolar, slender shape. In the cecum (D), ICC-MY (arrows) were multipolar-shaped. In the colon (E, F), ICC-SM (double arrowheads, E) and ICC-MY (arrows, F) were observed in the submucosal layer of the circular muscle and myenteric layer, respectively. Bar: 100 μm.

lature of W^{sh}/W^{sh} mice. In E18.5, in the small intestine (Fig. 6C and D), c-Kit immunoreactivity was only observed at the myenteric layer as ICC-MY in BALB/c mice, but there was no c-Kit immunoreactivity in the myenteric layer of W^{sh}/W^{sh} mice.

Discussion

In this study, we examined ICC in the GI musculature of W^{sh}/W^{sh} mice. We used an anti-c-Kit antibody to assess the cryosections and whole mounts and found that there were no c-Kit immunopositive cells in the GI musculature of W^{sh}/W^{sh} mice, in accordance with previous studies (7, 16). Our research used two antibodies
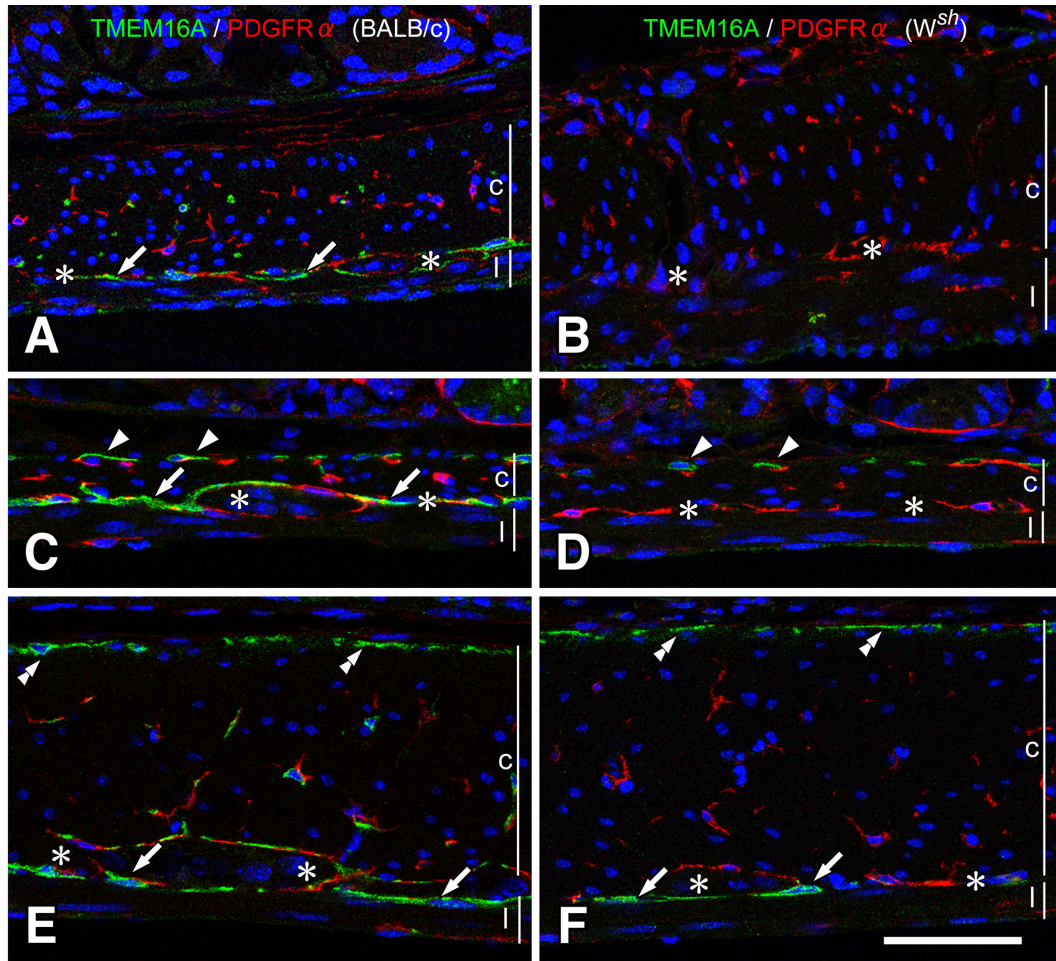
Fig. 4. ICC and FLC in BALB/c and W^{sh}/W^{sh} mice.
ICC and FLC were detected to have TMEM16A (green) and PDGFRα (red) immunoreactivities, respectively. In the stomach (A, B), small intestine (C, D), and proximal colon (E, F), ICC were observed only as restricted subtypes in W^{sh}/W^{sh} mice (B, D, F), whereas FLC were observed as being similar to that in BALB/c mice (A, C, E). ICC-DMP (arrowheads), ICC-SM (double arrowheads), and ICC-MY (arrows) were observed in W^{sh}/W^{sh} mice tissues. c and l represent circular and longitudinal muscle layers, respectively. Asterisks show myenteric layer. Bar: 50 μm.

ACK4 and AF1356, while Grimbaldeston report (7) used a different c-Kit antibody with the same results in the GI musculature of W^{sh}/W^{sh} mice. However, we previously demonstrated c-Kit immunonegative ICC in W^{sh}/W^{sh} mice's small intestine as ICC-DMP using NK1R, a specific marker for ICC-DMP (16). In the present study, we examined ICC using another marker, TMEM16A, recently known to be specifically expressed in ICC (17–19, 23), and identified several ICC types in W^{sh}/W^{sh} mice. ICC, characterized through TMEM16A as immunopositive and through c-Kit as immunonegative, were almost the same as the ICC in other W mutant mice that have been addressed by a number of studies (9, 10). Detectable ICC in both W^{sh}/W^{sh} and previously reported W mutant mice were identified as ICC-MY in the gastric corpus-antrum, cecum and colon, ICC-DMP in the small intestine, and ICC-SM in the colon (11, 20). Using an electron microscope, we also confirmed the ICC subtypes in each part of the GI musculature of W^{sh}/W^{sh} mice. We detected ICC-MY in the stomach and colon, ICC-DMP in the small intestine, and ICC-SM in the colon. The ultrastructure of ICC observed in W^{sh}/W^{sh} mice was in agreement with their previously reported characteristics: multiple mitochondria and caveolae and close contact with the nerve terminals (21, 26). By contrast, the lack of ICC subtypes was similar to the results of TMEM16A
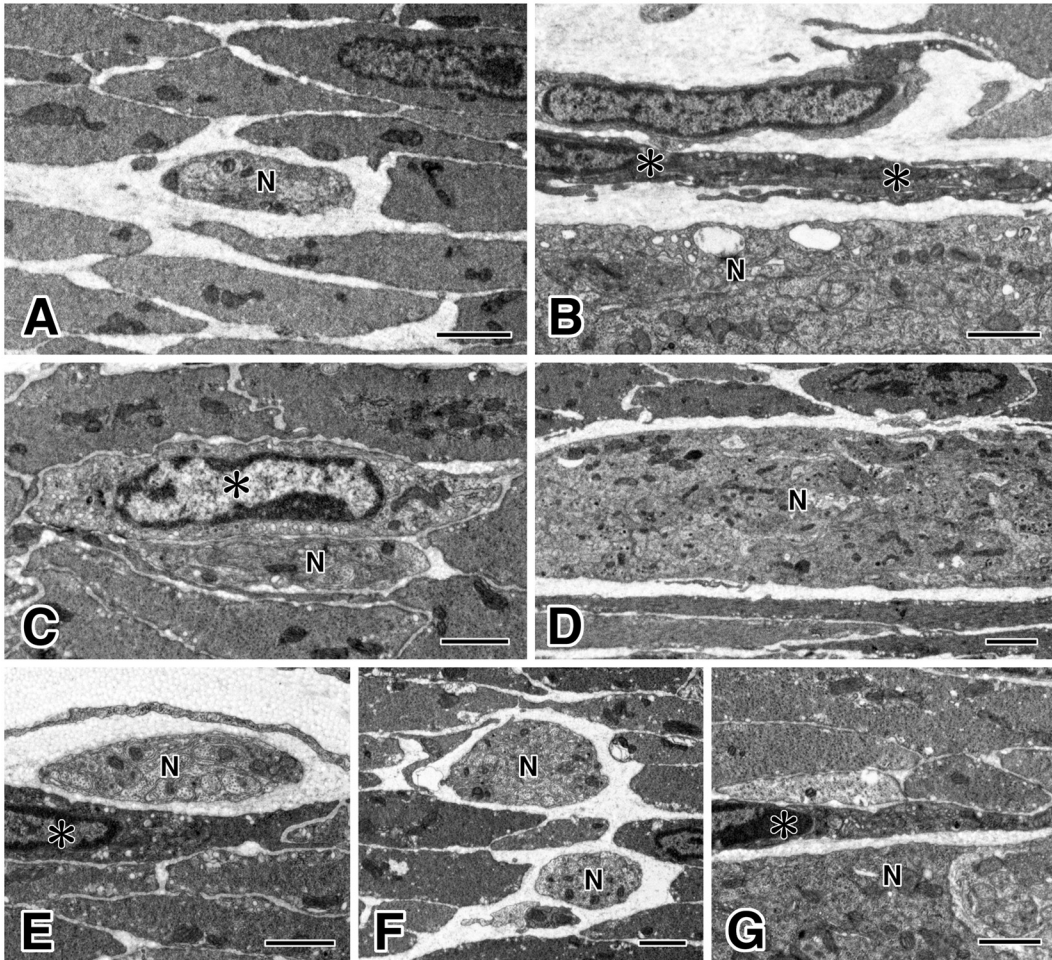
Fig. 5. Electron microscopic features of ICC in W^{sh}/W^{sh} mice.
In the gastric corpus (A, B), ICC-IM were not observed in the musculature; however, ICC-MY (asterisks in B) were observed with ICC features along the myenteric ganglion (N). In the small intestine (C, D), ICC-DMP (asterisk in C) were observed to be associated with nerve fiber bundles (N) in the circular muscle layer, but ICC-MY were not observed around the myenteric ganglion (N). In the proximal colon (E-G), ICC-SM (asterisk in E) were observed at the submucosal surface of the circular muscle, and ICC-MY (asterisk in G) were found around the myenteric ganglion (N). In the circular muscle (F), ICC-IM were not observed. Generally, smooth muscle cells, myenteric ganglia, and nerve fiber bundles (N) were observed to have normal structures. Bars: 2 μm (ABCEFG), and 5 μm (D).

immunohistochemistry, including the absence of ICC-IM in the stomach and colon and ICC-MY in the small intestine. From these findings, W^{sh}/W^{sh} mice have several ICC types that show c-Kit immunonegativity and TMEM16A immunopositivity and a typical cellular ultrastructure.

ICC development and differentiation are thought to depend on their c-Kit signaling. Therefore, loss of function mutations in the *c-kit* gene in *W* mutant mice, such as W/W^{v}, W^{v}/W^{v}, and W^{jic}/W^{jic}, and c-Kit ligand-SCF insufficiency in Sl/Sl^{d} mice caused developmental defects of the ICC subtypes (9–11, 20). However, c-Kit-signal-independent development has also been reported. From developmental studies in c-Kit-signal-insufficient mice, ICC-DMP were developed and differentiated to express both c-Kit and NK1R immunoreactivities postnatally to reveal their ultrastructure (15). Most of these findings were derived using *W* mutant animals that possessed weak c-Kit signaling and detectable c-Kit immunoreactivity. In the present W^{sh}/W^{sh} study, all ICC that were examined using the TMEM16A antibody showed immunonegativity for c-Kit and would appear to
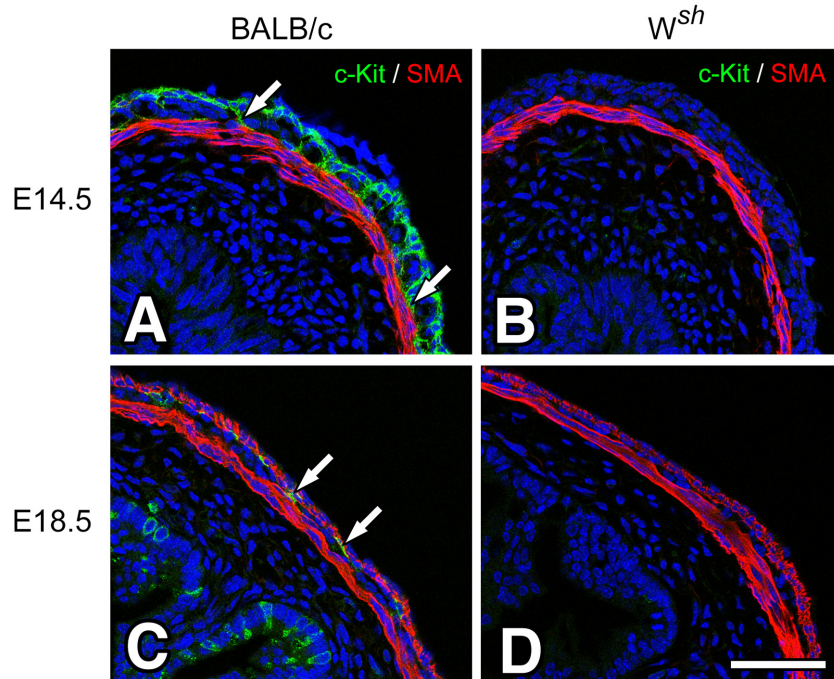
Fig. 6. Developmental changes of intestinal musculature in BALB/c and W^{sh}/W^{sh} mice. In embryos of both 14.5 (E14.5) and 18.5 (E18.5) days, the small intestine was observed using c-Kit ACK4 (green) and SMA (red) antibodies. In the BALB/c intestine (A, C), c-Kit immunopositive cells were clearly observed in the myenteric (arrows) and longitudinal layers in E14.5 (A) and myenteric layer (arrows) in E18.5 (C). In the small intestines of W^{sh}/W^{sh} mice (B, D), c-Kit immunoreactivity was not observed in both E14.5 (B) and E18.5 (D). The muscular structures of both mice stained with the SMA antibody appeared to be closely similar. Bar: 50 μm.

not have c-Kit signaling from the embryonic period to adulthood. In conjunction with previous reports, the ICC subtypes have the potential to develop and differentiate without c-Kit signaling. W^{sh}/W^{sh} mice have fewer defects and are fertile, making them different from other W mutants (6, 7); therefore, W^{sh}/W^{sh} mice are suitable as a model to investigate the unknown signaling on ICC development.

The calcium-activated chloride channel TMEM16A is expressed in smooth muscle cells in respiratory, urogenital, and vascular organs, but only in ICC in the GI tract (17). All ICC subtypes in humans and mice expressed TMEM16A and were specifically detected by TMEM16A immunoreactivity more than c-Kit immunoreactivity (23, 27). As Wang et al. (23) reported, TMEM16A immunohistochemistry is recommended over c-Kit immunohistochemistry to reveal all ICC subtypes in the mouse colon; hence, our study using TMEM16A immunohistochemistry showed all conceivable types of ICC in W^{sh}/W^{sh} mutant mice. In ICC, TMEM16A presumably performs a fundamental role in the pacemaker function (18, 19) and a possible role in regulating ICC proliferation (28). TMEM16A is expressed in the ICC tumor GIST (gastrointestinal stromal tumor) and is involved in regulating cancer growth and invasion (29). TMEM16A expression in ICC considerably suggests the proliferation potential of this molecule and TMEM16A has the potential to act as ICC proliferation instead of c-Kit signal in W^{sh}/W^{sh} mice. On the other hand, in the small intestine of TMEM16A knockout mice, ICC normally develop their structure at the neonatal stage (18, 30). Therefore, ICC proliferation signals in W^{sh}/W^{sh} mice are not related to TMEM16A signal and remains to be elucidated.

In conclusion, W^{sh}/W^{sh} mice have several ICC types that were both c-Kit immunonegative and TMEM16A immunopositive and may serve as a new model for investigating the effects of signaling on ICC development.

Conflict of Interest

The authors declare that they have no conflict of interest.

Acknowledgment

References

1. Chabot B, Stephenson DA, Chapman VM, Besmer P, Bernstein A. The proto-oncogene *c-kit* encoding a transmembrane tyrosine kinase receptor maps to the mouse W locus. Nature. 1988; 335(6185): 88–9. [Medline] [CrossRef]

2. Qiu FH, Ray P, Brown K, Barker PE, Jhanwar S, Ruddle FH, Besmer P. Primary structure of *c-kit*: relationship with the CSF-1/PDGF receptor kinase family--oncogenic activation of *v-kit* involves deletion of extracellular domain and C terminus. EMBO J. 1988; 7(4): 1003–11. [Medline] [CrossRef]

3. Lennartsson J, Jelacic T, Linnekin D, Shivakrupa R. Normal and oncogenic forms of the receptor tyrosine kinase kit. Stem Cells. 2005; 23(1): 16–43. [Medline] [CrossRef]

4. Sanders KM. A case for interstitial cells of Cajal as pacemakers and mediators of neurotransmission in the gastrointestinal tract. Gastroenterology. 1996; 111(2): 492–515. [Medline] [CrossRef]

5. Duttlinger R, Manova K, Berrozpe G, Chu TY, DeLeon V, Timokhina I, Chaganti RS, Zelenetz AD, Bachvarova RF, Besmer P. The W^{sh} and *Ph* mutations affect the *c-kit* expression profile: *c-kit* misexpression in embryogenesis impairs melanogenesis in W^{sh} and *Ph* mutant mice. Proc Natl Acad Sci USA. 1995; 92(9): 3754–8. [Medline] [CrossRef]

6. Lyon MF, Glenister PH. A new allele sash (W^{sh}) at the *W*-locus and a spontaneous recessive lethal in mice. Genet Res. 1982; 39(3): 315–22. [Medline] [CrossRef]

7. Grimbaldeston MA, Chen CC, Piliponsky AM, Tsai M, Tam SY, Galli SJ. Mast cell-deficient *W-sash c-kit* mutant *Kit* $^{W-sh/W-sh}$ mice as a model for investigating mast cell biology *in vivo*. Am J Pathol. 2005; 167(3): 835–48. [Medline] [CrossRef]

8. Iino S, Horiguchi K. Interstitial cells of Cajal are involved in neurotransmission in the gastrointestinal tract. Acta Histochem Cytochem. 2006; 39(6): 145–53. [Medline] [CrossRef]

9. Rumessen JJ, Vanderwinden JM. Interstitial cells in the musculature of the gastrointestinal tract: Cajal and beyond. Int Rev Cytol. 2003; 229: 115–208. [Medline] [CrossRef]

10. Sanders KM, Ward SM. Kit mutants and gastrointestinal physiology. J Physiol. 2007; 578(Pt 1): 33–42. [Medline] [CrossRef]

11. Iino S, Horiguchi S, Horiguchi K, Nojyo Y. Interstitial cells of Cajal in the gastrointestinal musculature of W mutant mice. Arch Histol Cytol. 2007; 70(3): 163–73. [Medline] [CrossRef]

12. Huizinga JD, Thuneberg L, Klüppel M, Malysz J, Mikkelsen HB, Bernstein A. *W/kit* gene required for interstitial cells of Cajal and for intestinal pacemaker activity. Nature. 1995; 373(6512): 347–9. [Medline] [CrossRef]

13. Ward SM, Burns AJ, Torihashi S, Sanders KM. Mutation of the proto-oncogene c-kit blocks development of interstitial cells and electrical rhythmicity in murine intestine. J Physiol. 1994; 480(Pt 1): 91–7. [Medline] [CrossRef]

14. Ward SM, Burns AJ, Torihashi S, Harney SC, Sanders KM. Impaired development of interstitial cells and

intestinal electrical rhythmicity in *steel* mutants. Am J Physiol. 1995; 269(6 Pt 1): C1577–85. [Medline] [CrossRef]

15. Iino S, Horiguchi K, Horiguchi S. c-Kit-stem cell factor signal-independent development of interstitial cells of Cajal in murine small intestine. Cell Tissue Res. 2020; 379(1): 121–9. [Medline] [CrossRef]

16. Iino S, Horiguchi K, Nojyo Y. *W^{sh}/W^{sh}* c-Kit mutant mice possess interstitial cells of Cajal in the deep muscular plexus layer of the small intestine. Neurosci Lett. 2009; 459(3): 123–6. [Medline] [CrossRef]

17. Huang F, Rock JR, Harfe BD, Cheng T, Huang X, Jan YN, Jan LY. Studies on expression and function of the TMEM16A calcium-activated chloride channel. Proc Natl Acad Sci USA. 2009; 106(50): 21413–8. [Medline] [CrossRef]

18. Hwang SJ, Blair PJA, Britton FC, O'Driscoll KE, Hennig G, Bayguinov YR, Rock JR, Harfe BD, Sanders KM, Ward SM. Expression of anoctamin 1/TMEM16A by interstitial cells of Cajal is fundamental for slow wave activity in gastrointestinal muscles. J Physiol. 2009; 587(Pt 20): 4887–904. [Medline] [CrossRef]

19. Gomez-Pinilla PJ, Gibbons SJ, Bardsley MR, Lorincz A, Pozo MJ, Pasricha PJ, Van de Rijn M, West RB, Sarr MG, Kendrick ML, Cima RR, Dozois EJ, Larson DW, Ordog T, Farrugia G. Ano1 is a selective marker of interstitial cells of Cajal in the human and mouse gastrointestinal tract. Am J Physiol Gastrointest Liver Physiol. 2009; 296(6): G1370–81. [Medline] [CrossRef]

20. Iino S, Horiguchi S, Horiguchi K. Interstitial cells of Cajal in the gastrointestinal musculature of *W^{jic}* *c-kit* mutant mice. J Smooth Muscle Res. 2011; 47(3-4): 111–21. [Medline] [CrossRef]

21. Horiguchi K, Komuro T. Ultrastructural observations of fibroblast-like cells forming gap junctions in the *W/W^v* mouse small intestine. J Auton Nerv Syst. 2000; 80(3): 142–7. [Medline] [CrossRef]

22. Iino S, Horiguchi K, Horiguchi S. Investigation of Novel c-Kit-expressing Smooth Muscle Cells in Murine Cecum. Acta Histochem Cytochem. 2020; 53(2): 11–9. [Medline] [CrossRef]

23. Wang XY, Chen JH, Li K, Zhu YF, Wright GW, Huizinga JD. Discrepancies between c-Kit positive and Ano1 positive ICC-SMP in the *W/W^v* and wild-type mouse colon; relationships with motor patterns and calcium transients. Neurogastroenterol Motil. 2014; 26(9): 1298–310. [Medline] [CrossRef]

24. Iino S, Horiguchi K, Horiguchi S, Nojyo Y. c-Kit-negative fibroblast-like cells express platelet-derived growth factor receptor alpha in the murine gastrointestinal musculature. Histochem Cell Biol. 2009; 131(6): 691–702. [Medline] [CrossRef]

25. Torihashi S, Ward SM, Sanders KM. Development of c-Kit-positive cells and the onset of electrical rhythmicity in murine small intestine. Gastroenterology. 1997; 112(1): 144–55. [Medline] [CrossRef]

26. Tamada H, Kiyama H. Existence of c-Kit negative cells with ultrastructural features of interstitial cells of Cajal in the subserosal layer of the *W/W^v* mutant mouse colon. J Smooth Muscle Res. 2015; 51: 1–9. [Medline] [CrossRef]

27. Loera-Valencia R, Wang XY, Wright GW, Barajas-López C, Huizinga JD. Ano1 is a better marker than c-Kit for transcript analysis of single interstitial cells of Cajal in culture. Cell Mol Biol Lett. 2014; 19(4): 601–10. [Medline] [CrossRef]

28. Mazzone A, Eisenman ST, Strege PR, Yao Z, Ordog T, Gibbons SJ, Farrugia G. Inhibition of cell proliferation by a selective inhibitor of the Ca^{2+}-activated Cl^- channel, Ano1. Biochem Biophys Res Commun. 2012; 427(2): 248–53. [Medline] [CrossRef]

29. Oh U, Jung J. Cellular functions of TMEM16/anoctamin. Pflugers Arch. 2016; 468(3): 443–53. [Medline] [CrossRef]

30. Singh RD, Gibbons SJ, Saravanaperumal SA, Du P, Hennig GW, Eisenman ST, Mazzone A, Hayashi Y, Cao C, Stoltz GJ, Ordog T, Rock JR, Harfe BD, Szurszewski JH, Farrugia G. Ano1, a Ca^{2+}-activated Cl^- channel, coordinates contractility in mouse intestine by Ca^{2+} transient coordination between interstitial cells of Cajal. J Physiol. 2014; 592(18): 4051–68. [Medline] [CrossRef]